BeBeC-2022-S09

# NUMERICAL COMPARISON OF ACOUSTIC IMAGING ALGORITHMS FOR A SPHERICAL MICROPHONE ARRAY

Kevin Rouard[1], Julien St-Jacques[1], Franck Sgard[2], Hugues Nélisse[2], Alain Berry[3]
Nicolas Quaegebeur[3], François Grondin[3], Olivier Doutres[1] and Thomas Padois[1]
[1]École de technologie supérieure (ÉTS)
1100 Rue Notre Dame O., Montréal, QC, H3C 1K3, Canada
[2]Institut de recherche Robert-Sauvé en santé et en sécurité du travail (IRSST)
505 Boulevard de Maisonneuve O., Montréal, QC, H3A 3C2, Canada
[3]Université de Sherbrooke (UdeS)
2500, Boulevard de l'Université, Sherbrooke, QC, J1K 2R1, Canada

**Abstract**

In a workplace, sound waves come from all directions. Spherical microphone arrays are therefore more suitable than planar microphone arrays to localize sources. If the microphones are flush-mounted on a solid sphere, the microphone array is considered rigid. Otherwise, the microphones can be mounted on a wireframe and the microphone array is said to be open. With a rigid spherical microphone array, the most efficient algorithm is the spherical harmonic beamforming (SHB) because the scattering effect can be considered. With an open spherical microphone array, beamforming can be performed in the frequency domain, known as conventional beamforming (CBF), or in the time domain based on the generalized cross-correlation (GCC). In this study a comparison of the three algorithms is conducted numerically for a point source located in a room. The room impulse response between the source and a spherical array, either rigid or open, is used to compute the acoustic pressure at the microphone positions. The acoustic images obtained with the different methods are characterized quantitatively by using a covariance ellipse to surround the main lobe and determine its area. The influence of the frequency of the source signal and the sphere radius on the obtained acoustic images is investigated.

## 1 INTRODUCTION

Many workers suffer from hearing loss due to exposure to excessive noise levels. Hearing protection is the simplest solution to safeguard workers' hearing, but its efficiency is limited [6]. The most efficient noise control solutions involve the elimination or the substitution of the source and the use of acoustic materials and barriers. Implementing these solutions may require to localize the noise source. This task can be performed with a spherical microphone array (SMA) which is more suitable than a planar microphone array to localize the acoustic sources in a workplace because it captures the sound waves coming from all directions. The result is an acoustic image where the source positions provided by the beamforming is overlaid on a picture of the workplace.

Acoustic imaging with SMA has been used with rigid or open design. The SMA is referred to as rigid when the microphones are flush-mounted on a solid sphere and open when the microphones are mounted on a wireframe. Rigid SMA can interfere with the acoustic waves and can induce scattering effects while open SMA is considered transparent with respect to the acoustic waves. In addition to this design difference, the sphere radius, the microphones number and position can vary. Moreover, acoustic images can be achieved with various beamforming algorithms.

In 2004, Petersen developed a rigid SMA with an optimized t-design geometry of 64 microphones and a radius of 14 cm. He evaluated the spherical harmonic beamforming (SHB) and the conventional frequency domain beamforming (CBF) algorithms [20]. In 2008, Haddad & Hald proposed an extension of the SHB to get an estimate of the source level, called spherical harmonics angularly resolved pressure (SHARP). They used a rigid SMA of 36 microphones with a radius of 9.75 cm [7]. In 2013, Hald increased the number of microphones to 50 with the same rigid SMA and presented the filter and sum algorithm to improve the side lobe rejection [8]. In 2016, Araujo compared the SHB and CBF in the case of a rigid SMA with 20 microphones and t-design geometry [1]. He showed, as Petersen, that the SHB provides a better resolution than the CBF at low frequencies [20, 1]. Classic deconvolution algorithms initially developed for planar microphone arrays have been adapted to the SHB with rigid SMA [2]. In 2019, Chu *et al.* used the same rigid SMA as Haddad & Hald. They tested a combination of SHARP with CLEAN and CLEAN-SC and found an improvement of acoustic images with CLEAN-SC algorithm [3].

In 2002, Merimaa presented a double open layer SMA of 12 microphones with a radius of 0.5 cm and 5 cm. He discussed the different applications possible with this SMA, such as room response measurement, sound recording or source localization [13]. In 2006, Noel proposed an open SMA of 15 microphones with a radius of 25 cm and used a time domain technique based on the generalized cross-correlation (GCC) [14]. In 2008, Heilmann *et al.* presented open SMAs with respectively 48 and 120 microphones with a time domain algorithm [9]. In 2016, Djordjevic *et al.* developed an open SMA of 32 microphones with a radius of 7.5 cm and used the SHB algorithm [4]. Padois *et al.* used two open SMAs, with a radius of 25 cm with 14 or 15 microphones. They used the GCC with geometric and energetic criteria for improving the acoustic images [19]. They also compared the geometrical or harmonic mean to the arithmetic mean for improving the acoustic images even with few microphones [16, 15]. In 2017, Du *et al.* evaluated open SMAs of 64 microphones with a radius of 15 cm and concluded that the best performance is given with the spiral geometry [5]. In 2019, Padois *et al.* proposed an optimized geometry for open SMA, with 18 microphones with a radius of 20 cm, based on the aperture angle of a microphone pair and the scan points [17].

Different microphone array geometries have been used in the literature. In 2005, Rafaely compared the equi-angle, Gauss's and t-design geometries for a rigid SMA and showed that the t-design generates the least spatial aliasing [22]. In 2016, Lecomte *et al.* compared the Lebedev's, t-design and Fliege's geometries and showed that the microphone distribution with Lebedev's geometry provides the best performance in terms of sound field capture and reproduction in ambisonic field [12]. In 2017, Du *et al.* compared several geometries such as t-design and spiral geometry. They concluded that spiral geometry gives the best performance of sound source localization with CBF and an open SMA [5]. The Lebedev's and spiral geometries have not been compared yet while the t-design geometry seems the most used.

This literature review has shown that various SMAs have been tested with different designs, radius, number of microphones, geometry and algorithm. The SMA design, the number of microphones and the radius are usually set and the investigations concern the optimization of the geometry or the algorithm. In this study a comparison of the three algorithms SHB, CBF and GCC is conducted numerically for a point source in a room and far enough from the SMA to consider plane waves. The t-design, Lebedev's and spiral are considered with rigid and open SMA. The theoretical background of these algorithms is introduced in section 2. The methodology is presented in section 3. The room impulse response (RIR) method is used to compute the acoustic pressure at the SMA. The selected geometries are depicted. The ellipse area criterion surrounding the main lobe or the side lobes is presented. Acoustic images obtained with the three algorithms and geometries are presented in section 4. The quantitative comparison, according to the algorithms, geometry, radius or frequency, is achieved with the ellipse area. The conclusions of this work is drawn in the last section 5.

## 2 THEORETICAL BACKGROUND

### 2.1 Frequency domain beamforming

Matrix and vector terms are denoted in bold. The common form of the acoustic image $\mathbf{A}$ in the frequency domain can be written as

$$\mathbf{A}(\omega) = \mathbf{w}^*(\omega)\mathbf{C}(\omega)\mathbf{w}(\omega), \tag{1}$$

where $\omega$ is the angular frequency, $\mathbf{w}$ is the matrix of weights and $\mathbf{C}$ is the cross-spectral matrix of the acoustic pressure given by

$$\mathbf{C}(\omega) = \mathbf{p}(\omega)\mathbf{p}^*(\omega), \tag{2}$$

where the vector $\mathbf{p}$ contains the sound pressure recorded at each microphone location and $(.)^*$ is the hermitian operator. The dimensions of $\mathbf{A}$, $\mathbf{w}$, $\mathbf{C}$ and $\mathbf{p}$ are $[L \times 1]$, $[Q \times L]$, $[Q \times Q]$ and $[Q \times 1]$ respectively, where $Q$ denotes the number of microphones and $L$ is the number of scan points of the acoustic image. The terms of $\mathbf{w}$ can differ according to the chosen algorithm, namely SHB or CBF. With a SMA, the matrix of the weights $\mathbf{w}$ scans over a grid of coordinate points $(\theta_l, \phi_l)$, where $l = 1, \ldots, L$ and $\theta_l$ and $\phi_l$ are the elevation and azimuth angles, respectively.

### 2.2 Spherical harmonic beamforming

The right terms of Eq. (1) are transformed into the spherical harmonic domain, respectively the modal matrix of weights, denoted $\mathbf{w}_{nm}$ of dimension $[(N+1)^2 \times L]$, and the modal pressure, denoted $\mathbf{p}_{nm}$ of dimension $[(N+1)^2 \times 1]$ where the index $n = 0, 1, \ldots, N$ is the order and index $m = -n, \ldots, n$ is the mode or degree. As proposed by Rafaely [24], the modal matrix of weights is

$$\mathbf{w}^*_{nm}(kr_a, \theta_l, \phi_l) = \mathbf{Y}^m_n(\theta_l, \phi_l)\frac{d_n}{\mathbf{b}_n(kr_a)}, \tag{3}$$

where $k$ is the wavenumber, $r_a$ is the sphere radius of the SMA, $d_n = 4\pi/(N+1)^2$ is a weight parameter giving the maximum directivity [23]. The spherical harmonic matrix $\mathbf{Y}^m_n(\theta_l, \phi_l)$ has a dimension of $[L \times (N+1)^2]$. The contribution of the amplitude of plane waves on the sphere, denoted by $\mathbf{b}_n$, is given by

$$\begin{cases} \mathbf{b}_n(kr_a) & = 4\pi\imath^n j_n(kr_a) & \rightarrow \text{open SMA}, \\ \mathbf{b}_n(kr_a) & = 4\pi\imath^n \left( j_n(kr_a) - \frac{j'_n(kr_a)}{h'^{(2)}_n(kr_a)} h^{(2)}_n(kr_a) \right) & \rightarrow \text{rigid SMA}, \end{cases} \tag{4}$$

where $\imath = \sqrt{-1}$ is the pure imaginary number, $j_n$ is the Bessel function of first kind, $h^{(2)}_n$ is the Hankel function of second kind. The operator $(.)'$ denotes the derivative of these functions with respect to $r$. The dimension of $\mathbf{b}_n$ is $[(N+1)^2 \times 1]$. The modal pressure is given by

$$\mathbf{p}_{nm}(kr_a, \theta_q, \phi_q) = \alpha_q \mathbf{Y}^{m^*}_n(\theta_q, \phi_q)\, \mathbf{p}(kr_a, \theta_q, \phi_q), \tag{5}$$

with $\alpha_q$ a weight which depends on the microphone positions on the sphere and $\mathbf{Y}^{m^*}_n(\theta_q, \phi_q)$ the spherical harmonic matrix with dimension $[(N+1)^2 \times Q]$. The spherical harmonic function is given by

$$Y^m_n(\theta, \phi) = \sqrt{\frac{2n+1}{4\pi}\frac{(n-m)!}{(n+m)!}} P^m_n(\cos\theta) e^{\imath m\phi}, \tag{6}$$

with $P^m_n$ the associated polynomial Legendre function. Note that $Y^{-m}_n$ is obtained by multiplying $Y^{m*}_n$ by the Condon-Shortley factor $(-1)^m$ [10].

### 2.3 Conventional beamforming

With the conventional beamforming, the matrix of the weights in the case of plane waves is given by

$$\mathbf{w}^*(\omega, \theta_l, \phi_l) = e^{\imath\vec{k}(\omega, \theta_l, \phi_l).\vec{\mathbf{r}}}, \tag{7}$$

where $\vec{\mathbf{r}}$ is the microphone positions and $\vec{k}(\omega, \theta_l, \phi_l)$ is the scan point directions.

### 2.4 Generalized cross-correlation

The cross-correlation $\mathrm{R}_{uv}(\tau)$ estimates the time delay between two microphone signals $(u,v)$ and can be obtained by the inverse Fast Fourier Transform of the cross-spectrum $C_{uv}$

$$\mathrm{R}_{uv}(\tau) = \sum_{j=0}^{N_f-1} C_{uv}(\omega_j) e^{\imath \omega_j \tau / N_f}, \tag{8}$$

where $\tau$ is the time lag, $j$ is a discrete frequency and $N_f$ the number of elements of the frequency vector. The acoustic image is provided by the arithmetic mean of the projected cross-correlations [21]

$$\mathbf{A}(\theta_l, \phi_l) = \frac{1}{Q_p} \sum_{p=1}^{Q_p} \mathrm{R}_{uv}(\tau_{uvl}) \tag{9}$$

where $\tau_{uvl} = \Delta t_{ul} - \Delta t_{vl}$ is the difference of the time delays for each microphone $(u,v)$ and scan point location $l$. The arithmetic mean is performed over the $Q_p = Q(Q-1)/2$ microphone pairs.

## 3 METHODOLOGY

### 3.1 Simulation of the sound field recorded by a SMA

To compare the algorithms, numerical simulations in the time domain are performed. The RIR developed by Jarret *et al.* is used to get the microphone signals over a rigid or open SMA [11]. A room with dimensions $18 \times 12 \times 5$ m$^3$ is considered, respectively width, length and height. The reflection coefficient of the room walls is 0.01 to approximate anechoic conditions. The frequency sampling is $f_s = 65,536$ Hz and the sound speed is $c_0 = 343$ m/s. The SMA is at the center of the room, considered as ($x_0 = 9$ m,$y_0 = 6$ m,$z_0 = 2.5$ m). The source is positioned at ($r_s = 4$ m,$\theta_s = 90°, \phi_s = 0°$). The source signal is a sine wave. The RIR is convolved with the source signal to obtain the microphone signals on the SMA. The scan zone is a grid of $90 \times 180$ points distributed along the elevation angle $\theta_l \in [0°, 180°]$ and azimuth $\phi_l \in [-180°, 180°]$.

### 3.2 Microphone array geometry

The t-design, Lebedev's and spiral geometries are considered in this study. These geometries are shown on a sphere and plotted in the $(\theta, \phi)$ plane in Fig. 1. A number of 48 microphones is chosen for the t-design geometry. It corresponds to a high polynomial order $t = 9$ for a minimum number of microphones. The t-design geometry has a constant weight value given by $\alpha_q = 4\pi/Q$. A number of 48 microphones cannot be obtained with Lebedev's geometry. Instead, the number of microphones is set to the closest to 48, namely 50 microphones. A number of 48 microphones for the spiral distribution is chosen for the comparison.

The truncation order of the spherical harmonics is set to $N = 4$ for all geometries. The SMA radius is set to $r_a = 0.1$ m for the rigid SMA, in low and high frequencies, and varies from $r_a = 0.1, 0.2$ to 0.3 m for the open SMA in low frequency and is set to $r_a = 0.1$ m for the last frequency case.

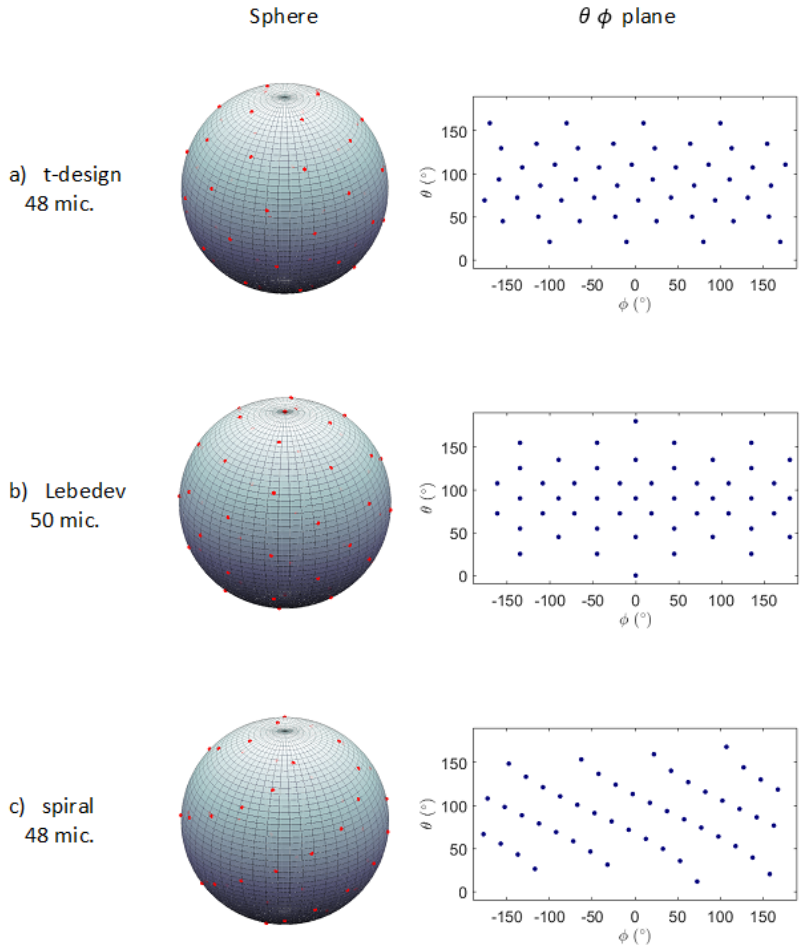


*Figure 1: Microphone array of t-design, Lededev's and spiral geometries depicted on sphere and $(\theta, \phi)$ plane.*

### 3.3 Acoustic image criterion

The method of the ellipse area at $-3$ dB and $-9$ dB is used to compare the acoustic images [18]. An example is shown in Fig. 2 where the ellipses are depicted on the acoustic image obtained with an open SMA with a frequency *a)* $f = 1,716$ Hz and *b)* $f = 3,000$ Hz. The position of the true source is depicted by a green cross. The ellipse radii at $-3$ dB and $-9$ dB are obtained by the covariance matrix method. The ellipse areas, referred to as $S_{-3\,\mathrm{dB}}$ or $S_{-9\,\mathrm{dB}}$, are obtained by multiplying the radii of the ellipses. The ellipse area is then normalized by the largest possible radii that corresponds to the limits of the acoustic image, such as $90^\circ \times 180^\circ$. Therefore, the computed area is an arbitrary unit (a.u.). Note that the ellipse areas $S_{-3,-9\,\mathrm{dB}} \geq 1$ a.u. extend beyond the frame of the acoustic image, meaning a poor source localization. At the opposite, low values of $S_{-3,-9\,\mathrm{dB}}$ suggest an efficient localization. When the main lobe is well defined, the ellipse area at $-3$ dB attempts to give a similar information to the main lobe width. The ellipse area at $-9$ dB attempts to provide a similar information than the side lobe level.

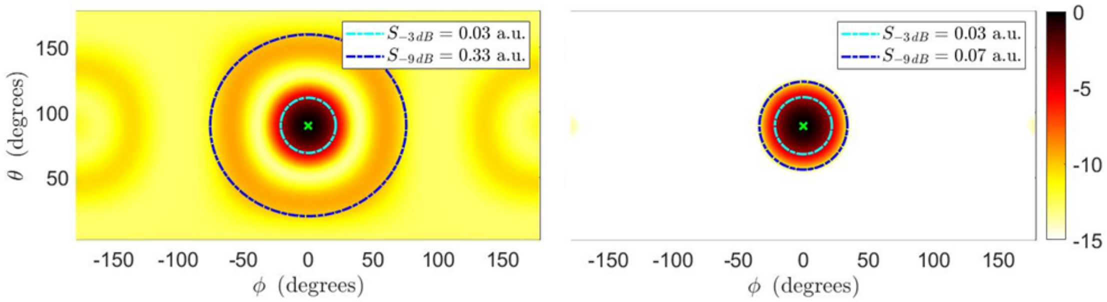


a) $f$ = 1,716 Hz b) $f$ = 3,000 Hz

*Figure 2: Acoustic images provided by an open SMA with 48 microphones with t-design geometry - $r_a = 0.1$ m. The dashed cyan and blue lines defined the ellipse areas at $-3$ dB and $-9$ dB, respectively. The green cross exhibits the true source position.*

## 4 ACOUSTIC IMAGES RESULTS

The three algorithms are compared with different SMA. Low and high frequency source signals are considered to highlight the performance of each algorithm. With the rigid SMA, the cases at 500 Hz and $3,000$ Hz are shown in Figs. 3-4. With the open SMA, the cases at 500 Hz and $1,715$ Hz are shown in Figs. 5-6. The acoustic images obtained with the three algorithms are arranged in columns corresponding to the algorithms, while the rows refer to the geometry, radius or frequency.

### 4.1 Rigid SMA at 500 Hz

The acoustic images obtained at 500 Hz with the rigid SMA are shown in Fig. 3. The acoustic images given by the CBF and GCC algorithms are similar, irrespective of the geometry considered and confirm the previous findings [18]. The CBF and GCC algorithms provide similar ellipse areas, $S_{-3\text{ dB}} = 0.54$ a.u. and $S_{-9\text{ dB}} = 1.51$ a.u. for each geometry, except in the case of the Lebedev's geometry where the ellipse area value is slightly larger, *i.e.* $S_{-9\text{ dB}} = 1.52$ a.u.. The CBF and GCC ellipse areas are too wide to consider that the source is correctly identified. The acoustic images obtained with the SHB algorithm depend on the geometry. First, the t-design geometry allows to identify the source with no side lobes in the acoustic image, $S_{-3\text{ dB}} = 0.03$ a.u. and $S_{-9\text{ dB}} = 0.07$ a.u.. The Lebedev's geometry can identify the source with the lowest ellipse area at $-3$ dB, $S_{-3\text{ dB}} = 0.02$ a.u., but with the presence of side lobes in the acoustic image, $S_{-9\text{ dB}} = 1.54$ a.u.. The spiral geometry cannot localize the source. The values of the ellipse areas are $S_{-3\text{ dB}} = 1.25$ a.u. and $S_{-9\text{ dB}} = 1.46$ a.u.. In conclusion, for a low frequency source signal, the SHB outperforms the CBF and GCC, but is highly dependent on the geometry considered.

### 4.2 Rigid SMA at $3,000$ Hz

The acoustic images obtained at $3,000$ Hz with a rigid SMA are shown in Fig. 4. The CBF and GCC algorithms produced the same results with each geometry, the ellipse areas are $S_{-3\text{ dB}} =$

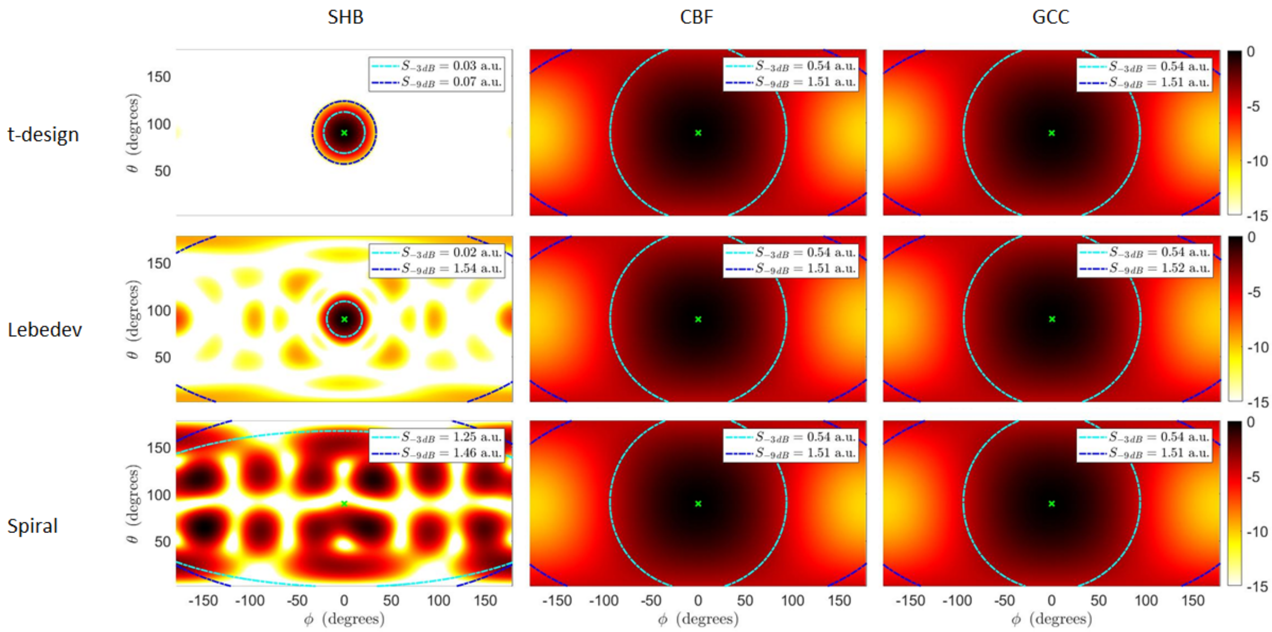


*Figure 3: Acoustic images provided by a rigid SMA with t-design, Lebedev's and spiral geometry and with the SHB, CBF and GCC algorithms – $r_a = 0.1$ m and $f = 500$ Hz. The dashed cyan and blue lines defined the ellipse areas at $-3$ dB and $-9$ dB, respectively. The green cross exhibits the true source position.*

0.01 a.u. and $S_{-9\text{ dB}} = 0.03$ a.u.. The ellipse areas obtained with the aforementioned algorithms are smaller than those obtained with the SHB algorithm; $S_{-3\text{ dB}} = 0.03$ a.u. and $S_{-9\text{ dB}} = 0.07$ a.u.. The acoustic image obtained with the SHB algorithm and the spiral geometry has side lobes below $-9$ dB compared to the t-design and Lebedev's geometry. Note that with the SHB algorithm and t-design geometry the area at $-3$ dB in Fig. 3-4 are identical which is in agreement with the results presented by Petersen and Araujo [20, 1]. In conclusion, when the frequency of the source signal increases, the CBF and GCC become better than the SHB.

### 4.3 Open SMA at 500 Hz

The acoustic images obtained at 500 Hz with an open SMA and only a t-design geometry is shown in Fig. 5. Three radii of $r_a = 0.1, 0.2$ and $0.3$ m are considered. The ellipse areas obtained with the CBF and GCC algorithms are identical for a given radius. When the radius increases, the ellipse areas decrease such as $S_{-3\text{ dB}} = 1.28 > 0.16 > 0.07$ a.u. and $S_{-9\text{ dB}} = 1.53 > 0.44 > 0.17$ a.u.. The ellipse areas with the largest radius $r_a = 0.3$ m show a better localization of the source than with the smallest radius $r_a = 0.1$ m. The SHB algorithm leads to a constant ellipse area whatever the radius, $S_{-3\text{ dB}} = 0.03$ a.u. and $S_{-9\text{ dB}} = 0.07$ a.u.. Moreover, the ellipse areas are identical with the t-design geometry and the SHB algorithm whether the open and rigid SMA (Fig. 3); $S_{-3\text{ dB}} = 0.03$ a.u. and $S_{-9\text{ dB}} = 0.07$ a.u.. With the CBF and GCC algorithms, the ellipse areas are smaller with the rigid SMA (Fig. 3) and t-design geometry than the open SMA design, such as $S_{-3\text{ dB}} = 0.54 < 1.28$ a.u. and $S_{-9\text{ dB}} = 1.51 < 1.53$ a.u.. In conclusion, when the radius of the SMA increases, acoustic images of the CBF and GCC are

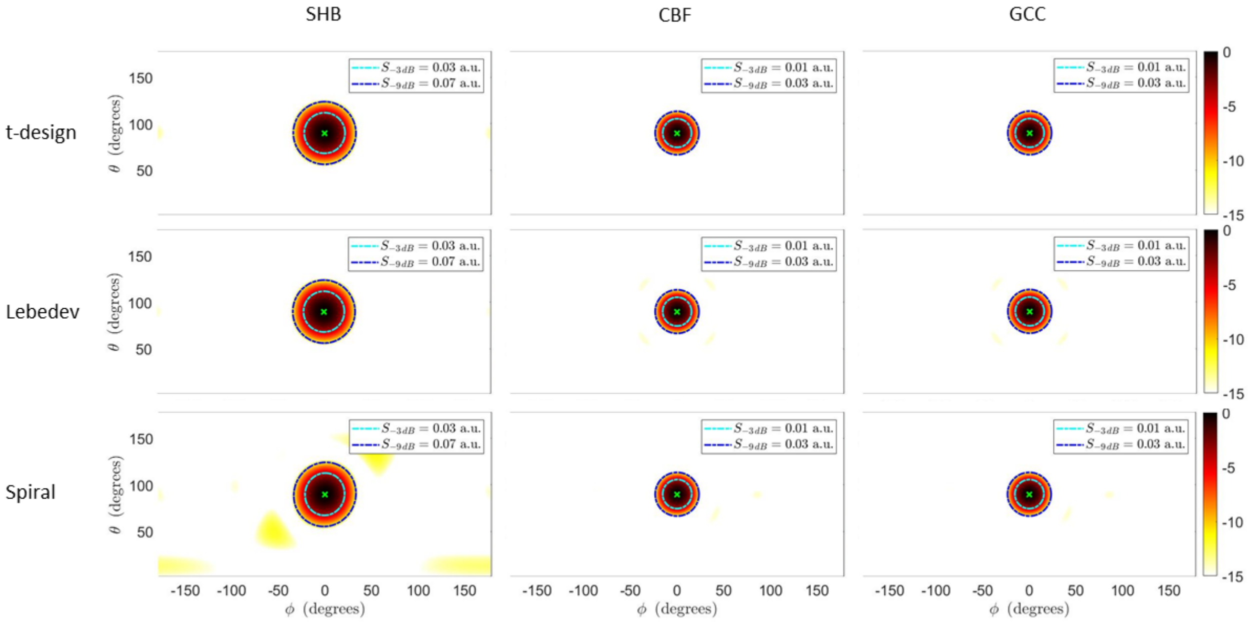


*Figure 4: Acoustic images provided by a rigid SMA with t-design, Lebedev's and spiral geometry and with the SHB, CBF and GCC algorithms – $r_a = 0.1$ m and $f = 3,000$ Hz. The dashed cyan and blue lines defined the ellipse areas at $-3$ dB and $-9$, respectively. The green cross exhibits the true source position.*

improved. Nevertheless, the SHB outperforms the CBF and GCC.

### 4.4 Open SMA at $1,715$ Hz

One issue with an open SMA and the SHB is the zero of the Bessel function (Eq. (4)). For the first degree $n = 0$, these frequency values correspond to $kr_a = l\pi$ where $l$ is an integer number. The numerical application for $l = 1$ gives $f = c/2r_a = 1,715$ Hz. The acoustic images obtained at this frequency $1,715$ Hz with an open SMA of radius $r_a = 0.1$ m and a t-design geometry are shown in the first row of Fig. 6. Acoustic images obtained with CBF and GCC give identical ellipse areas, $S_{-3\text{ dB}} = 0.03$ a.u. and $S_{-9\text{ dB}} = 0.07$ a.u.. As expected, the SHB gives an erroneous acoustic image due to the divergent calculation from the zero the Bessel function. The associated ellipse area values are $S_{-3,-9\text{ dB}} = 1.53$ a.u.. The acoustic images obtained in the frequency range of 1 700 Hz to 1 730 Hz centered at the problematic frequency are shown in the second row of Fig. 6. Acoustic images obtained with the CBF and GCC remain identical and acoustic images obtained with SHB give a correct result. In conclusion, the problematic frequency corresponding to the zero of the Bessel function can be smoothed in a frequency band.

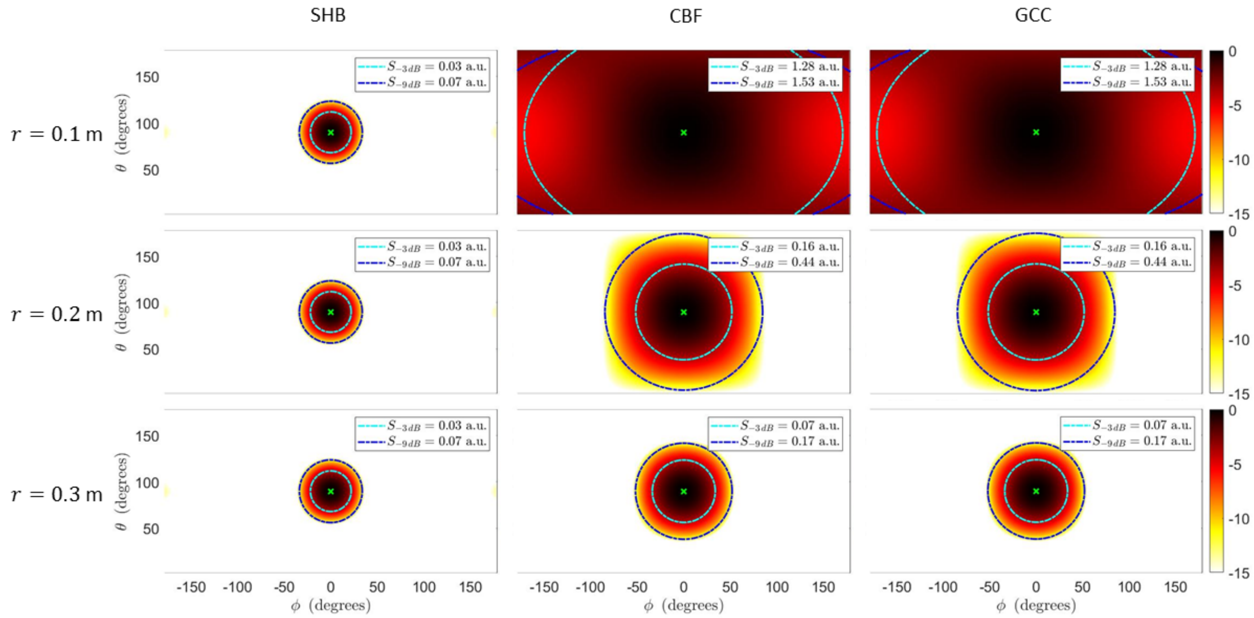


*Figure 5: Acoustic images provided by an open SMA with 48 microphones with t-design geometry and with the SHB, CBF and GCC algorithms – $r_a = 0.1, 0.2$ and $0.3$ m, $f = 500$ Hz. The dashed cyan and blue lines defined the ellipse areas at $-3$ dB and $-9$ dB, respectively. The green cross exhibits the true source position.*

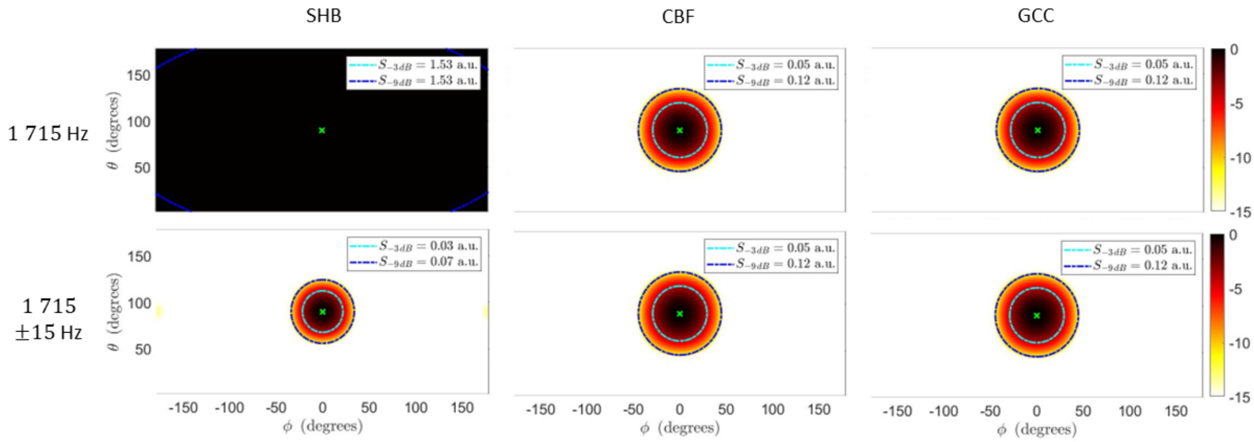


*Figure 6: Acoustic images provided by an open SMA with 48 microphones with t-design geometry and with the SHB, CBF and GCC algorithms – $r_a = 0.1$ m, $f = 1{,}715$ Hz and $1{,}715 \pm 15$ Hz. The dashed cyan and blue lines defined the ellipse areas at $-3$ dB and $-9$ dB, respectively. The green cross exhibits the true source position.*

## 5 Conclusion

This preliminary work deals with a numerical comparison of acoustic imaging algorithms for spherical microphone arrays (SMA). Two designs are considered, *i.e.* rigid and open, with three microphone geometries, namely t-design, Lebedev and spiral. The algorithms selected are the spherical harmonic beamforming (SHB), the conventional beamforming (CBF) and the generalized cross-correlation (GCC). The influence of the source signal frequency and the SMA radius are investigated. The numerical simulation of an anechoic room without added noise to the acoustic pressure signal is performed. The criterion used for comparing the acoustic images is based on the ellipse areas at $-3$ dB and $-9$ dB.

The results show that the SHB has constant ellipse areas at $-3$ dB and $-9$ dB with the t-design geometry. While the Lebedev's geometry allows for reducing the ellipse area at $-3$ dB in low frequency, the ellipse areas at $-9$ dB is the widest, which means higher side lobe level. The spiral geometry does not provide efficient source localization with SHB. With this algorithm and the t-design geometry, it shows that the radius has no-influence for the selected cases. Finally, it shows that the SHB fails to localize the source position when the source signal frequency is exactly at the zero of the Bessel function. However, if a larger frequency range is considered, the source position is well localized.

The CBF and GCC provide similar results no matter the SMA configuration. The smallest ellipse areas are obtained with the highest frequency source signal and the largest radius. Although the scattering effect, due to a rigid SMA, is not considered, both algorithms show similar behavior as already shown with planar microphone array.

In conclusion, SHB has the advantage of providing a small ellipse area at low frequencies while CBF and GCC provide a better result at high frequencies. Therefore, it could be interesting to optimize a SMA where it would be possible to select the best algorithm to consider or to combine them in order to improve the acoustic image while considering a computationally inexpensive algorithm. More complex conditions can also be studied such as reverberate room and noise to the acoustic pressure signal.

## References


[1] F. H. D. Araujo. “Comparison Between the Spherical Harmonics Beamforming and the Delay-and-Sum Beamforming.” In *INTER-NOISE and NOISE-CON Congress and Conference Proceedings*, volume 253, pages 1007–1017. Hamburg, 2016.

[2] Z. Chu, Y. Yang, and Y. He. “Deconvolution for Three-Dimensional Acoustic Source Identification Based on Spherical Harmonics Beamforming.” *Journal of Sound and Vibration*, 344, 484–502, 2015. URL `https://doi.org/10.1016/j.jsv.2015.01.047`.

[3] Z. Chu, S. Zhao, Y. Yang, and Y. Yang. “Deconvolution Using CLEAN-SC for Acoustic Source Identification with Spherical Microphone Arrays.” *Journal of Sound and Vibration*, 440, 161–173, 2019. URL `https://doi.org/10.1016/j.jsv.2018.10.030`.

[4] A. Djordjevic and M. Licanin. “Construction, Calibration, Evaluation of Spherical Microphone Array and its Application for Beamforming.” In *INTER-NOISE and NOISE-CON Congress and Conference Proceedings*, pages 4598–4609. Hamburg, 2016.

[5] C. Du, Q. Leclere, and B. Li. “Design and Evaluation of Open Spherical Microphone Arrays.” In *24th International Congress on Sound and Vibration*. London, 2017. URL `https://hal.archives-ouvertes.fr/hal-01595873`.

[6] M. R. Groenewold, E. A. Masterson, C. L. Themann, and R. R. Davis. “Do Hearing Protectors Protect Hearing?” *American Journal of Industrial Medicine*, 57(9), 1001–1010, 2014. URL `https://doi.org/10.1002/ajim.22323`.

[7] K. Haddad and J. Hald. “3D Localization of Acoustic Sources with a Spherical Array.” In *Acoustics' 08*, pages 1585–1590. Paris, 2008. URL `https://doi.org/10.1121/1.2933754`.

[8] J. Hald. “Spherical Beamforming with Enhanced Dynamic Range.” *SAE International Journal of Passenger Cars - Mechanical Systems*, 6(2), 1334–1341, 2013. URL `https://doi.org/10.4271/2013-01-1977`.

[9] G. Heilmann, A. Meyer, and D. Döbler. “Beamforming in the Time-domain using 3D-microphone Arrays.” In *XIXth Biennial Conference of the New Zealand Acoustical Society*. Auckland, 2008.

[10] D. P. Jarrett, E. A. P. Habets, and P. A. Naylor. “Chap. 2 - Theoritical Preliminaries of Acoustics.” In *Theory and Applications of Spherical Microphone Array Processing*, volume 9 of *Springer Topics in Signal Processing*. Springer International Publishing, Cham, 2017. ISBN 978-3-319-42209-1. doi:10.1007/978-3-319-42211-4. URL `http://doi.org/10.1007/978-3-319-42211-4`.

[11] D. P. Jarrett, E. A. P. Habets, M. R. P. Thomas, and P. A. Naylor. “Rigid Sphere Room Impulse Response Simulation: Algorithm and Applications.” *The Journal of the Acoustical Society of America*, 132(3), 1462–1472, 2012. URL `https://doi.org/10.1121/1.4740497`.

[12] P. Lecomte, P.-A. Gauthier, C. Langrenne, A. Berry, and A. Garcia. "A Fifty-Node Lebedev Grid and Its Applications to Ambisonics." *Journal of the Audio Engineering Society*, 64(11), 868–881, 2016. URL `http://dx.doi.org/10.17743/jaes.2016.0036`.

[13] J. Merimaa. "Applications of a 3-D Microphone Array." In *Audio Engineering Society Convention 112*. Munich, 2002.

[14] C. Noël, V. Planeau, and D. Habault. "A new Temporal Method for the Identification of Source Directions in a Reverberant Hall." *Journal of Sound and Vibration*, 296(3), 518–538, 2006. URL `https://doi.org/10.1016/j.jsv.2005.12.056`.

[15] T. Padois. "Acoustic Source Localization Based on the Generalized Cross-correlation and the Generalized Mean with few Microphones." *The Journal of the Acoustical Society of America*, 143(5), EL393–EL398, 2018. URL `https://doi.org/10.1121/1.5039416`.

[16] T. Padois, O. Doutres, F. Sgard, and A. Berry. "On the use of Geometric and Harmonic Means with the Generalized Cross-correlation in the Time Domain to Improve Noise Source Maps." *The Journal of the Acoustical Society of America*, 140(1), EL56–EL61, 2016. URL `https://doi.org/10.1121/1.4955007`.

[17] T. Padois, O. Doutres, F. Sgard, and A. Berry. "Optimization of a Spherical Microphone array Geometry for Localizing Acoustic Sources using the Generalized Cross-correlation Technique." *Mechanical Systems and Signal Processing*, 132, 546–559, 2019. URL `https://doi.org/10.1016/j.ymssp.2019.07.010`.

[18] T. Padois, J. Fischer, C. Doolan, and O. Doutres. "Acoustic Imaging with Conventional Frequency Domain Beamforming and Generalized Cross-correlation: a comparison study." *Applied Acoustics*, 177, 107914, 2021. URL `https://doi.org/10.1016/j.apacoust.2021.107914`.

[19] T. Padois, F. Sgard, O. Doutres, and A. Berry. "Acoustic Source Localization using a Polyhedral Microphone Array and an Improved Generalized Cross-correlation Technique." *Journal of Sound and Vibration*, 386, 82–99, 2017. ISSN 0022460X. doi:10.1016/j.jsv.2016.09.006. URL `https://linkinghub.elsevier.com/retrieve/pii/S0022460X16304527`.

[20] S. O. Petersen. "Localization of Sound Sources usign 3D Microphone Array." M.Sc. Eng. Thesis, University of Southern Denmark, 2004. URL `http://www.oscarpetersen.dk/speciale/Thesis.pdf`.

[21] N. Quaegebeur, T. Padois, P. A. Gauthier, and P. Masson. "Enhancement of time-domain acoustic imaging based on generalized cross-correlation and spatial weighting." *Mechanical Systems and Signal Processing*, 75, 515–524, 2016. URL `https://doi.org/10.1016/j.ymssp.2015.12.012`.

[22] B. Rafaely. "Analysis and Design of Spherical Microphone Arrays." *IEEE Transactions on Speech and Audio Processing*, 13(1), 135–143, 2005. URL https://doi.org/10.1109/TSA.2004.839244.

[23] B. Rafaely. "Phase-Mode versus Delay-and-Sum Spherical Microphone Array Processing." *IEEE Signal Processing Letters*, 12(10), 713–716, 2005. URL https://doi.org/10.1109/LSP.2005.855542.

[24] B. Rafaely. "Chap. 5 - Spherical Array Beamforming." In *Fundamentals of Spherical Array Processing*, number 16 in Springer Topics in Signal Processing, pages 103–126. Springer International Publishing : Imprint: Springer, Cham, 2nd ed. 2019 edition, 2019. ISBN 978-3-319-99561-1. URL https://doi.org/10.1007/978-3-319-99561-8.